Liquid-to-liquid crossover in the GaIn eutectic alloy

Q. Yu,[1] X. D. Wang,[1,*] Y. Su,[1] Q. P. Cao,[1] Y. Ren,[2] D. X. Zhang,[3] and J. Z. Jiang[1,†]

[1]*International Center for New-Structured Materials (ICNSM), Laboratory of New-Structured Materials, State Key Laboratory of Silicon Materials, and School of Materials Science and Engineering, Zhejiang University, Hangzhou 310027, People's Republic of China*

[2]*Advanced Photon Source, Argonne National Laboratory, Argonne, Illinois 60439, USA*

[3]*State Key Laboratory of Modern Optical Instrumentation, Zhejiang University, Hangzhou 310027, People's Republic of China*

(Received 13 January 2017; revised manuscript received 3 May 2017; published 6 June 2017)

Liquid-liquid crossover is promising and closely related to the atomic dynamics during heating and cooling processes. Here we reveal a reversible structural crossover in the liquid $Ga_{85.8}In_{14.2}$ eutectic alloys by using *in situ* synchrotron x-ray diffraction and *ab initio* molecular dynamics simulation. A kink always appears on the temperature dependent behaviors of density, ratio of the second peak position to the first in the pair correlation function, coordination number, heat capacity, free energy, and atomic diffusivity in the temperature range of about 400–550 K. It is likely ascribed to atomic rearrangements of Ga and In atoms from a relative random packing at high temperatures to a relative nonuniform packing at low temperatures, in which In atoms prefer to have more In neighbors. This observation will promote more understanding of the liquid structure of eutectic alloys.

DOI: 10.1103/PhysRevB.95.224203

I. INTRODUCTION

The temperature-induced liquid-to-liquid transition (LLT) is a long-standing issue from both experimental and theoretical points of view [1–16]. For instance, for liquid silicon, evidence indicated the existence of first-order LLT in the supercooled state [14–18], where two distinct regions with a high density liquid (HDL) and a low density liquid (LDL) were predicated by Aptekar [19]. The LLT was also observed in P [20,21], C [22,23], SiO_2 [12,24], $Al_2O_3-Y_2O_3$ [6,7], and molecular systems, e.g., water [8,9,25,26] and triphenyl phosphite [3–5,27]. Recently, few studies on LLT in metallic liquids Ce [28], $Zr_{41.2}Ti_{13.8}Cu_{12.5}Ni_{10}Be_{22.5}$ [11], $Zr_{58.5}Cu_{15.6}Ni_{12.8}Al_{10.3}Nb_{2.8}$ [13], and $La_{50}Al_{35}Ni_{15}$ [10] were carried out, which raised some basic questions of liquid melts, e.g., what atomic configurations they have, how they evolve with temperature, etc. Here we report the results of liquid-to-liquid crossover for a liquid $Ga_{85.8}In_{14.2}$ eutectic alloy, which has a low melting point of 288.3 K, studied by using *in situ* synchrotron x-ray diffraction (XRD) and *ab initio* molecular dynamics (AIMD) simulation. The experimental data clearly reveal a reversible structural crossover with a noticeable change in density at the temperature range from 400 to 550 K. Accordingly, the temperature dependent behaviors of partial coordination number (CN) of In atoms, heat capacity, free energy, atomic diffusivity, and diffusion activation energy were also detected during liquid-to-liquid crossover. This finding sheds light on the origin of LLT and implies that it could be a common phenomenon in some other metallic liquids.

The $Ga_{85.8}In_{14.2}$ eutectic alloy has a broad temperature range (~2000 K) of liquid state as well as promising potential in advanced applications [29–34], including liquid-metal nanomedicine, three-dimensional printing, liquid coolants, heat transfer fluids, self-healing circuits, and printed electronics. However, so far, only a few studies have been reported concerning the temperature dependent structure or dynamics in the liquid $Ga_{85.8}In_{14.2}$ alloy. The electronic magnetic susceptibility and Knight shift (K_s) of the $Ga_{85.8}In_{14.2}$ alloy were measured, and the different temperature dependence was detected between the supercooled liquid and the normal liquid state [35]. Yu and Kaviany studied the atomic structure and transport properties of liquid $Ga_{85.8}In_{14.2}$ alloy using AIMD [36]. Also, Zhao *et al.* [37] found the abnormal decrease in the nearest neighbor coordination number with decreasing temperature in the normal and undercooled liquid $Ga_{85.8}In_{14.2}$ alloy. Liquid structures and viscosities of GaIn alloys with different compositions were measured [38], but unfortunately, the abovementioned studies were limited to low temperatures less than 500 K, and the atomic level structure has been rarely studied.

II. EXPERIMENTAL AND THEORETICAL METHODS

A. *In situ* high-temperature, high-energy x-ray diffraction

The sample $Ga_{85.8}In_{14.2}$ eutectic alloy used in the present paper was prepared by melting high purity Ga (99.99%) and In (99.99%) and then sealing it into a 1.5-mm-diameter quartz capillary under a vacuum of $\sim 8.6\times10^{-4}$ Pa. The *in situ* high-temperature, high-energy XRD measurements were carried out at the beamline 11-ID-C at the Advance Photon Source, Argonne National Laboratory, Argonne, Illinois. The x-ray beam size used was $\sim 0.8\times0.8$ mm^2 with a wavelength of 0.11798 Å. The sealed capillary was fixed in a Linkam TS1500 furnace perpendicular to the incoming beam. The heating and cooling rate was 10 K/min. Upon heating/cooling, the diffraction patterns were *in situ* automatically collected from 300 K by a flat panel Si detector (Perkin Elmer 1621) with 200×200 μm^2 pixel size and 2048 × 2048 pixels. Exposure time was 1 s, and 20 diffraction patterns were summed for each data set. Background was recorded by measuring an empty capillary in the same setup. Two-dimensional diffraction patterns were integrated after subtracting the background in the software package FIT2D [39]. The total structure factor $S(q)$ was obtained after standard corrections by removing the effects of self-absorption, polarization, fluorescence absorption, and

*wangxd@zju.edu.cn

†Corresponding author: jiangjz@zju.edu.cn

Compton scattering using PDFgetX3 [40]. Subsequently, the pair distribution function $G(r)$ was obtained through Fourier transform of $S(q)$.

B. Thermal expansion measurements

The linear thermal expansion of the liquid $Ga_{85.8}In_{14.2}$ alloy was measured using a Netzsch DIL 402 C pushrod dilatometer, which has been proved appropriate for measuring the thermal expansion and density of condensed solids and liquids [41–44]. The liquid samples were sealed into a well-designed sample holder and pushed by two pistons with a constant load of 0.15 N during the experiment. The sample length change was detected by a displacement transducer with 1.25 nm precision, and the temperature was monitored by thermocouples located at the lateral surface of the sample. All measurements were carried out under a pure Ar atmosphere with a flow rate of 60 ml/min, and the sample was heated from room temperature to 1000 K at a rate of 5 K/min. The measurements were carried out four times to reduce systematic errors and to guarantee the accuracy of data. Before experiments, the setup was calibrated by using a 10 mm length of Al_2O_3 rod and a pure Sn standard sample for testing the expansion measurement. The density of the liquid melt can be evaluated using the method given in Ref. [42].

C. Molecular dynamics simulations

The AIMD simulation of the $Ga_{86}In_{14}$ alloy was performed based on the density functional theory (DFT) by using the Vienna *Ab initio* Simulation Package (VASP) [45], combined with a canonical NVT ensemble and Nosé-Hoover thermostat for temperature control [46]. The projector augmented wave (PAW) method with the generalized gradient approximation (GGA) of Perdew and Wang [47,48] was adopted to describe the electronic exchange and correlation functions. The Newton's equation of motion was simulated using the velocity Verlet algorithm with a typical time step of 3 fs. Only the Γ

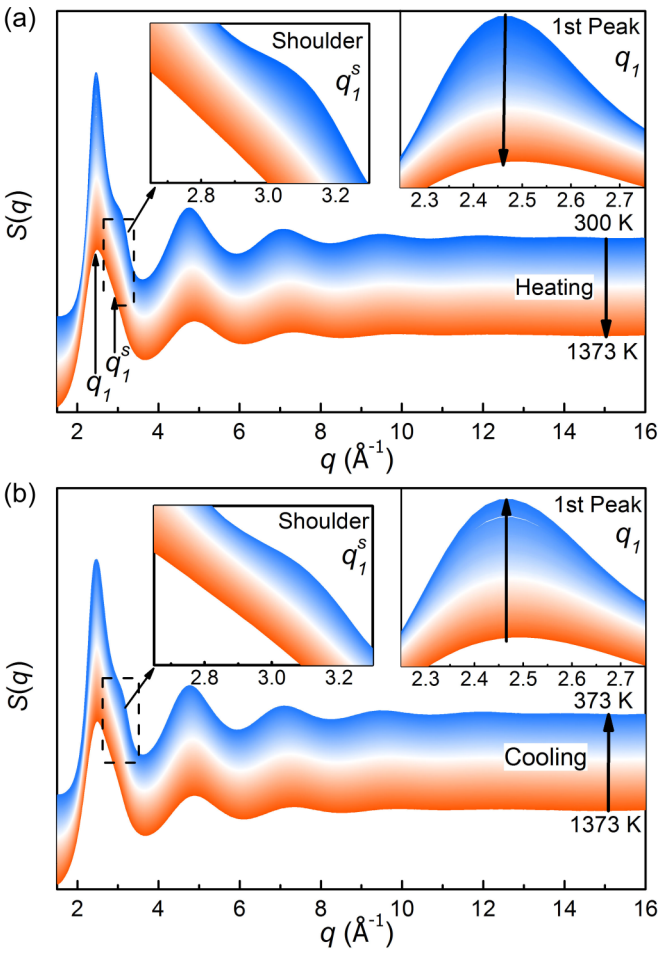

FIG. 1. Total structure factor $S(q)$ during (a) heating from 300 to 1373 K and (b) cooling from 1373 to 373 K obtained from *in situ* synchrotron XRD for liquid $Ga_{85.8}In_{14.2}$ eutectic alloy. Arrows in (a) indicate the main component (q_1) and shoulder (q_1^s) of the first peak in $S(q)$. The insets display local magnifications of the first peak. As the temperature decreases, the principal peak (q_1) in $S(q)$ has a gradually pronounced shoulder (q_1^s) by an enlarged view in the left inset.

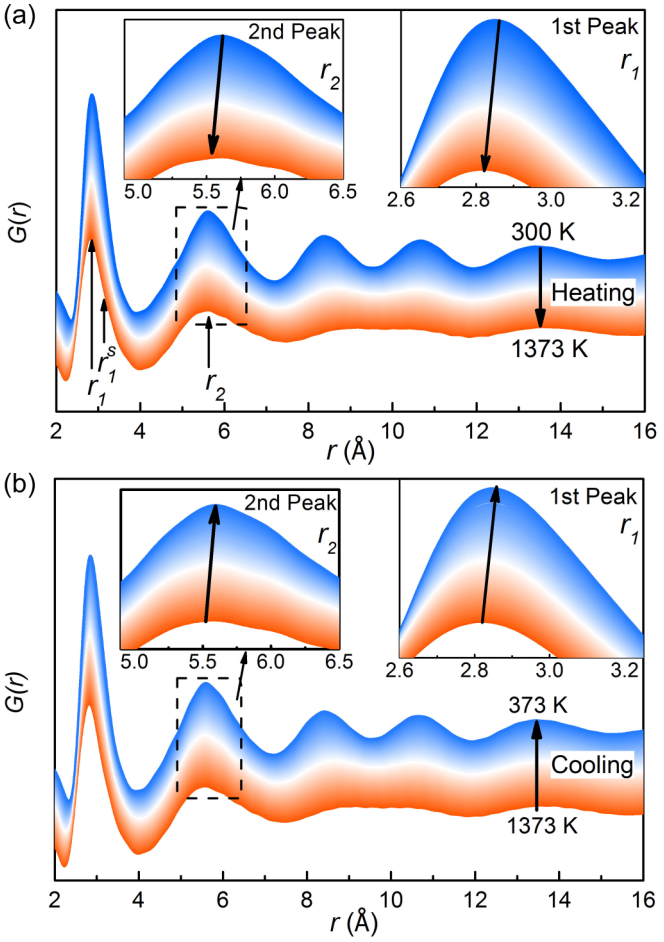

FIG. 2. Reduced total pair distribution function $G(r)$ obtained by Fourier transformation from $S(q)$ in Fig. 1. (a) During heating from 300 to 1373 K and (b) upon cooling from 1373 to 373 K in the liquid $Ga_{85.8}In_{14.2}$ eutectic alloy. The right and left insets represent the local magnifications of the first and second peaks of $G(r)$, respectively. The arrows show the principal peaks (r_1 and r_2) as well as the small subpeak (r_1^s) separated from the first main peak. With the decrease of temperature, the first and second peak positions shift towards higher r values.

point was used to sample the Brillouin zone of the supercell. An initial random box consisting of 250 atoms (215 Ga and 35 In) with periodic boundary conditions was melted and thermally equilibrated at 1500 K for more than 6000 time steps to remove the memory effect of the initial configuration, then quenched in steps to 1200, 1000, 900, 800, 700, 650, 600, 550, 500, 450, 400, 350, and 300 K with a cooling rate of 0.1 K/step. At each temperature, the equilibrium configurations could be achieved by adjusting the size of the simulation box to keep the external pressure close to zero pressure after 2000 time steps. Afterwards, additional equilibration of 10 000 time steps was performed, and the last 4000 configurations were collected for statistical analyses.

III. RESULTS AND DISCUSSION

Total structure factors $S(q)$ and pair distribution functions $G(r)$ of liquid $Ga_{85.8}In_{14.2}$ eutectic alloy obtained from *in situ* XRD over the entire heating and cooling cycle are plotted in Figs. 1 and 2, respectively. It exhibits a complex structure characterized by a shoulder at the high q side of the first peak in $S(q)$ in Fig. 1. To illustrate the evolution of these characteristic parameters with temperature, we apply two Gaussian functions to fit the first peak of $S(q)$ as shown in Fig. 3(a), similar fitting procedures were also reported in the literature [49–51]. It reveals that the two fitting curves can match the diffraction data well at both high and low temperatures. With increasing temperature, the first principal peak position (q_1) in $S(q)$ slightly shifts towards lower q value with the gradually reduced shoulder position ($q_1{}^s$). These changes are reversible during the cooling process. By carefully examining the first peak (insets) of $G(r)$ in Fig. 2, it is asymmetric and could be decomposed into two sub-Gaussian peaks [see Fig. 3(a)], i.e., the main component r_1 and shoulder $r_1{}^s$ marked by arrows in Fig. 2. The insets are local magnifications of the first two peaks in $G(r)$, showing that r_1 and r_2 both shift towards lower r values with increasing temperature. Again these changes are reversible during the cooling process. To better examine temperature dependent structural evolution, the principal peak positions ($q_1, q_1{}^s, r_1, r_1{}^s, r_2$) in $S(q)$ and $G(r)$ together with corresponding ratios ($q_1{}^s/q_1, r_1{}^s/r_1, r_2/r_1$) in both heating and cooling processes are plotted in Fig. 3(b). It is noted that the second peak positions in both $S(q)$ and $G(r)$ are derived by Gaussian fitting. The structural change is nearly reversible with heating and cooling processes, and the first peak positions ($q_1, q_1{}^s$) of $S(q)$ increase linearly with decreasing temperature, while the shoulder $q_1{}^s$ starts to deviate from the linear relation after a turning point at around 500 K. The structural change is more pronounced in the temperature dependence of $q_1{}^s/q_1$ in the range of 400 to 550 K identified by a pink rectangle. As the temperature decreases, the ratio $q_1{}^s/q_1$ declines linearly from high temperature to the turning point (~550 K) and presents an abrupt increase with a continuous rise in slope from 550 to 400 K. Examining the variation of peak positions in $G(r)$ curves, it is observed that the first main peak positions r_1 shifts linearly to high r value with decreasing temperature while the shoulder positions $r_1{}^s$ together with the ratio of $r_1{}^s/r_1$ decrease almost linearly above 500 K and become much steeper after 500 K. In general, a detailed study of the pair distribution function, especially beyond the first shell, is essential for

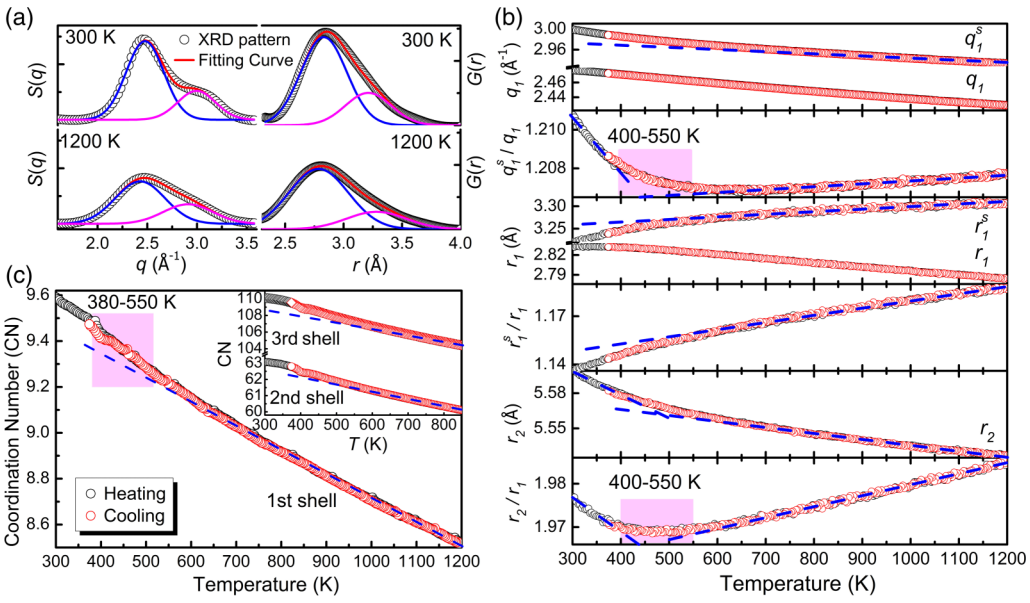

FIG. 3. Temperature dependent structural evolutions associated with LLT in the liquid $Ga_{85.8}In_{14.2}$ eutectic alloy. (a) Deconvolution of the first peak in $S(q)$ and $G(r)$ by using two Gaussian profiles at two selected temperatures of 300 and 1200 K, respectively. The open black circles represent the XRD diffraction data, the red curve the total fitting results, and the magenta and blue curves the two Gaussian peaks, respectively. The baseline is corrected before fitting. (b) The principal peak positions of $S(q)$ and the first two peak positions of $G(r)$, as well as their corresponding variations in ratios of $q_1{}^s/q_1$ and r_i/r_1 on heating and cooling processes for the liquid $Ga_{85.8}In_{14.2}$ eutectic alloy. Error bars are smaller than the symbol size. (c) The change of the nearest neighbor coordination number as a function of temperature in the liquid $Ga_{85.8}In_{14.2}$ eutectic alloy. The pink rectangle indicates a drop of CN in the temperature interval of 380–550 K. Similar drops exist in the second and third shell atoms, as shown in the right inset with varying temperature.

better understanding of structural changes of liquid $Ga_{85.8}In_{14.2}$ eutectic alloy. Therefore, taking the second peak position r_2 into consideration, it reveals the same trend as that of r_1, except for a temperature inflection at about 500 K, and the ratio of r_2/r_1 exhibits almost the same feature as the sudden change observed in ${q_1}^s/q_1$; i.e., both decline slowly first to a minimum, then rise again with decreasing temperature. These results indicate that the temperature dependent local atomic structure below the temperature range of about 400–550 K differs from that above this temperature range. To further investigate the atomic structural evolution, the experimental nearest neighbor CN as a function of temperature is depicted in Fig. 3(c). It can be seen that with increasing temperature, the CN of the first shell decreases linearly, and a drop (or a pronounced deviation from the linear relation) starts at ~380 K, then reverts to the linear relationship of temperature above ~550 K. Similar phenomena are also identified in the second and third shells, as shown in the right inset of Fig. 3(c), suggesting that the local structure, including not only the short-range order but also the intermediate-length scale, can be attributed to these structural changes. It is well known that CN values depend on the cutoff. In fact, here five different cutoff values were used; the observed features of the temperature dependent CN in Fig. 3(c) always appear.

To find out the underlying mechanism of experimental evidence of structural change in liquid $Ga_{85.8}In_{14.2}$ eutectic alloy, local structure and dynamic behaviors for liquid $Ga_{86}In_{14}$ alloy are further studied by AIMD calculations. Figures 4(a) and 4(b) display a set of the calculated pair correlation functions $g(r)$ and $S(q)$ during cooling, respectively, which show good agreement with the available experimental data in terms of shapes, peak positions, and amplitudes at the different temperatures, providing reasonable atomic configurations for further structural analyses. The Voronoi tessellation method [52,53] was performed to determine the nearest neighboring CN, in which the three-dimensional space is divided into various polyhedral cells constructed by a center atom and its nearest neighbors. The total number of faces on the Voronoi polyhedron is equivalent to the CN of the central atom. The total CN of the first shell, calculated by averaging all the atoms as well as the partial CNs around Ga and In atoms changing with temperature, are given in Fig. 4(c). The calculated total CN almost linearly decreases with increasing temperature, then suddenly drops at ~500 K, which likely corresponds to the 400 K drop detected by experiments in Fig. 3(b). It is clearly seen that partial CNs around In and Ga atoms exhibit different variation trends with increasing temperature. At ~550 K the number of Ga around Ga decreases from about 11 to 10, while Ga around In increases from about 8 to 10. In contrast, In around In decreases from about 4.5 to 2, and In around Ga increases from about 1 to 2. Above ~550 K, the temperature dependent partial CNs for both Ga-centered and In-centered polyhedra are similar. These results strongly imply that the local environments around Ga and In atoms below ~550 K are distinctly different from those around Ga and In atoms above ~550 K, which are getting similar at high temperatures. The local bond orientational order parameters Q_4 [54] for both Ga and In atoms based on spherical harmonics are shown in the inset of Fig. 4(c), both also revealing an evident crossover at ~600 K. All these results obtained from AIMD calculations

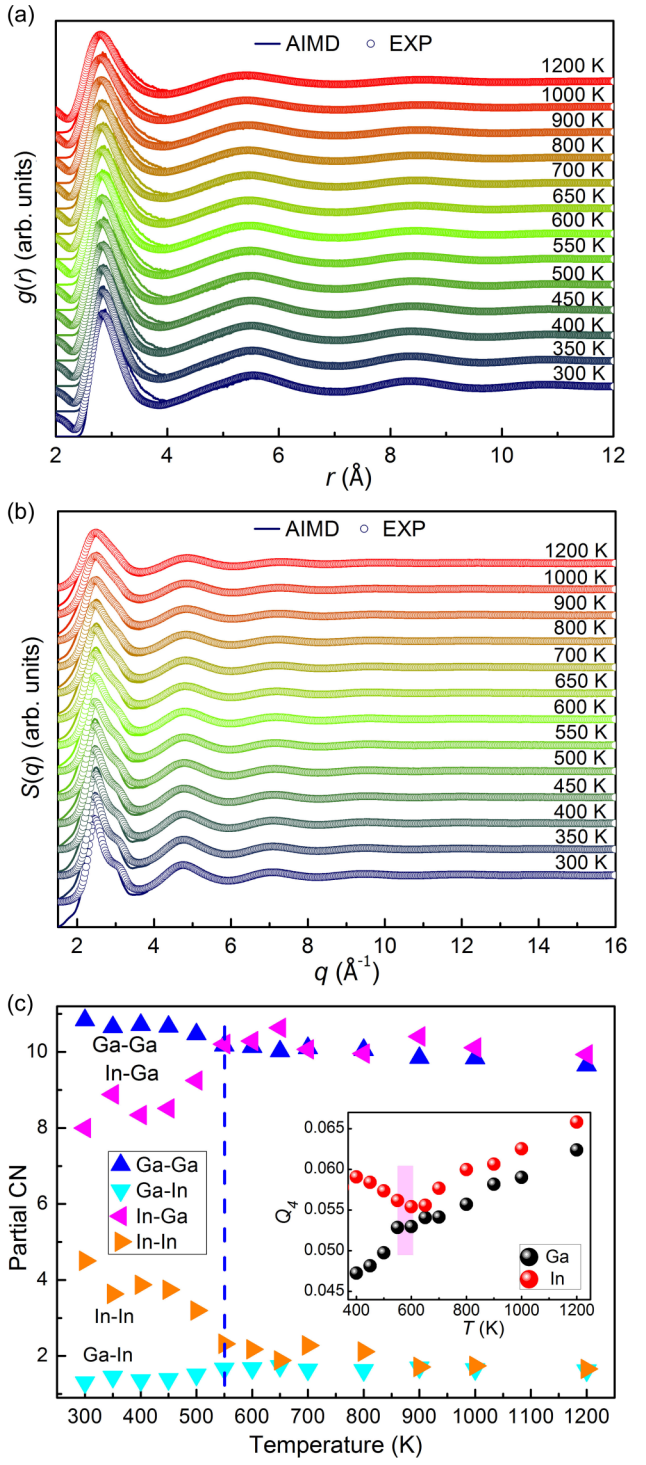

FIG. 4. Results obtained from *ab initio* molecular dynamic calculations for the liquid $Ga_{86}In_{14}$ alloy. Theoretical (a) $g(r)$ and (b) $S(q)$ compared with experimental data at different temperatures in the liquid GaIn alloy. The solid lines represent the AIMD curves and the circles for the experimental data. (c) The total coordination numbers for all atoms and partial coordination numbers for Ga-centered and In-centered Voronoi polyhedra in the liquid $Ga_{86}In_{14}$ alloy at various temperatures. The inset of panel (c) shows temperature dependences of the local bond orientational order parameter Q_4 of the individual elements. The vertical light pink region represents an abrupt change in atomic local symmetry, indicating a liquid-to-liquid crossover at the vicinity of 550 K.

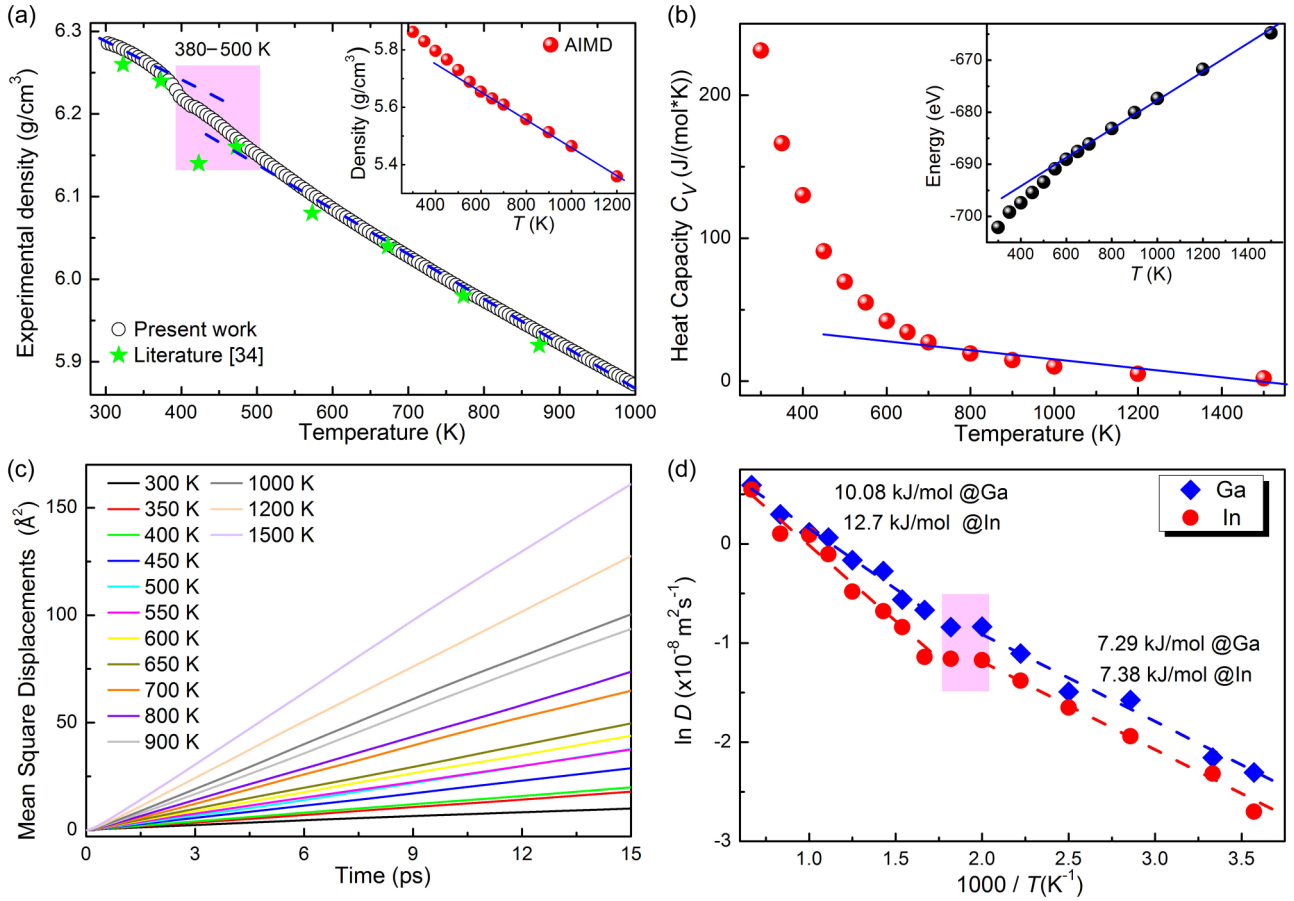

FIG. 5. Physical and thermodynamic properties of the liquid GaIn alloy as a function of temperature. (a) The experimental density measured by the dilatometer method in this paper (open circles) together with the reported experimental data obtained from Ref. [34] (green stars). For comparison, theoretical densities (red spheres) of the liquid $Ga_{86}In_{14}$ alloy obtained by AIMD in this paper are shown in the inset. (b) The heat capacity C_V versus temperature of the liquid $Ga_{86}In_{14}$ alloy calculated by AIMD simulations. The inset shows total free energy of the liquid $Ga_{86}In_{14}$ alloy upon cooling. The blue lines are only to guide the eyes and imply a deviation from the high-temperature linear relationship at around 600 K. (c) Time dependence of the mean square displacement (MSD) of liquid $Ga_{86}In_{14}$ during cooling. (d) The self-diffusion coefficients D, for Ga and In atoms as a function of temperature in the liquid $Ga_{86}In_{14}$ alloy. Activation energy changes are obvious for both elements at the vicinity of 550 K, in particular for In atoms.

indeed support the experimental observations in Figs. 3(b) and 3(c), confirming the existence of liquid-to-liquid crossover in the liquid $Ga_{85.8}In_{14.2}$ eutectic alloy.

It is reasonable to believe that the liquid-to-liquid crossover in liquid $Ga_{85.8}In_{14.2}$ eutectic alloy could reflect from its physical and thermodynamic properties. Figure 5(a) shows the temperature dependent density of this liquid measured by dilatometer during heating together with the experimental data from the literature [34] and the theoretical density obtained by AIMD here. Our experimental density data matched the reported experimental data well. It is clearly seen that a drop in density exists at ~400 K marked by a pink rectangle, consistent with the variation of CNs detected by XRD in Figs. 3(b) and 3(c). From AIMD calculations in the inset of Fig. 5(a), a deviation from the high-temperature linear relationship of density at ~550 K is clearly detected. Although some differences are observed in both experimental and theoretical density, the reduction rate of density obtained by AIMD in the high-temperature region is almost the same as that by experiment. Figure 5(b) shows the temperature dependent heat capacity C_V calculated by AIMD [55], revealing an abrupt increase below ~600 K and a temperature insensitive heat capacity C_V of the liquid $Ga_{86}In_{14}$ alloy above ~600 K. The total free energy versus temperature of the liquid $Ga_{86}In_{14}$ alloy is also plotted in the inset of Fig. 5(b), which displays a deviation at ~550 K from the high-temperature linear relationship of the total free energy of the system. The temperature dependences of self-diffusion coefficients D for Ga and In atoms were estimated from the mean square displacement (MSD) of atoms based on the Stokes-Einstein relation [56], in which time limit $t \to \infty$ corresponds to the diffusion coefficient D ($D = \mathrm{MSD}/t$). Figure 5(c) shows the calculated MSD as a function of time in liquid GaIn alloy at different temperatures. The linear dependence of the MSD with time reveals that the equilibrium configurations are generated *via* AIMD simulations. As a result, the diffusion coefficient D of Ga and In subtracted by averaging the last 6 ps in Fig. 5(c) are plotted in Fig. 5(d). The slopes are calculated to determine the activation energy using the Arrhenius equation. The liquid alloy exhibits two different diffusion regions separated by a transition region of ~500–600 K. For Ga, In atoms, the activation energy changes from 7.3 and 7.4 kJ/mol at the low-

temperature range (below ∼550 K) to 10.1 and 12.7 kJ/mol at the high-temperature region (above ∼550 K), respectively. It should be noted that activation energies of both Ga and In atoms at high temperatures are higher than those at low temperatures, which contradicts common sense that in uniform liquids the higher the temperature, the faster the atoms diffuse. The anomalous behavior of activation energies for both In and Ga atoms in the liquid $Ga_{86}In_{14}$ alloy also reflects the structure difference above and below the temperature region of ∼500–600 K, validating the existence of the liquid-to-liquid crossover in the liquid $Ga_{85.8}In_{14.2}$ eutectic alloy.

In summary, *in situ* high-temperature and high-energy XRD measurements provide experimental evidence on the existence of a reversible structural crossover in the liquid $Ga_{85.8}In_{14.2}$ eutectic alloy. It is found that below and above the temperature interval of about 400–550 K, the major peak positions of $S(q)$ and $G(r)$, as well as coordination number, vary in different ways. Particularly, ${q_1}^s/q_1$ and r_2/r_1 decrease with decreasing temperature but invert to a rapid increase below 400–600 K. Thermal expansion measurements of the liquid $Ga_{85.8}In_{14.2}$ eutectic alloy indicates an abrupt decline in density upon heating at the turning point around 380 K. The AIMD simulations can reproduce the liquid-to-liquid crossover phenomenon and reveal the structural change in the liquid $Ga_{86}In_{14}$ alloy. With decreasing temperature, the repulsive interaction between heteroatomic bonds becomes strong, i.e., Ga-In/In-Ga, by which In atoms prefer to have more In neighbors. Accordingly, the temperature dependences of the heat capacity, free energy, and atomic diffusivity also show different behaviors below and above the temperature range of liquid-to-liquid crossover. This finding will trigger more studies on liquids and be beneficial for the understanding of the nature of LLT.

ACKNOWLEDGMENTS

Financial support from the national natural science foundation (No. 51371157, U1432105, U1432110, U1532115, 51671170, and 51671169), the National Key Research and Development Program of China (No. 2016YFB0701203 and 2016YFB0700201), the Natural Science Foundation of Zhejiang Province (No. Z1110196 and Y4110192), and the Fundamental Research Funds for the Central Universities are gratefully acknowledged. The computer resources at National Supercomputer Centers in Tianjin and Guangzhou are also gratefully acknowledged. The beam time support at 11-ID-C of the Advance Photon Source, Argonne National Laboratory, is also greatly appreciated.

[1] P. H. Poole, T. Grande, C. A. Angell, and P. F. McMillan, Science **275**, 322 (1997).
[2] H. Tanaka, Phys. Rev. E **62**, 6968 (2000).
[3] M. Kobayashi and H. Tanaka, Nat. Commun. **7**, 13438 (2016).
[4] R. Kurita and H. Tanaka, Science **306**, 845 (2004).
[5] H. Tanaka, R. Kurita, and H. Mataki, Phys. Rev. Lett. **92**, 025701 (2004).
[6] S. Aasland and P. F. Mcmillan, Nature **369**, 633 (1994).
[7] G. N. Greaves, M. C. Wilding, S. Fearn, D. Langstaff, F. Kargl, S. Cox, Q. V. Van, O. Majerus, C. J. Benmore, R. Weber, C. M. Martin, and L. Hennet, Science **322**, 566 (2008).
[8] K. Ito, C. T. Moynihan, and C. A. Angell, Nature **398**, 492 (1999).
[9] F. Mallamace, M. Broccio, C. Corsaro, A. Faraone, D. Majolino, V. Venuti, L. Liu, C. Y. Mou, and S. H. Chen, Proc. Natl. Acad. Sci. USA **104**, 424 (2007).
[10] W. Xu, M. T. Sandor, Y. Yu, H. Ke, H. Zhang, M. Li, W. Wang, L. Liu, and Y. Wu, Nat. Commun. **6**, 7696 (2015).
[11] S. Wei, F. Yang, J. Bednarcik, I. Kaban, O. Shuleshova, A. Meyer, and R. Busch, Nat. Commun. **4**, 2083 (2013).
[12] I. Saika-Voivod, P. H. Poole, and F. Sciortino, Nature **412**, 514 (2001).
[13] M. Stolpe, I. Jonas, S. Wei, Z. Evenson, W. Hembree, F. Yang, A. Meyer, and R. Busch, Phys. Rev. B **93**, 014201 (2016).
[14] S. Sastry and C. Austen Angell, Nat. Mater. **2**, 739 (2003).
[15] N. Jakse and A. Pasturel, Phys. Rev. Lett. **99**, 205702 (2007).
[16] M. Beye, F. Sorgenfrei, W. F. Schlotter, W. Wurth, and A. Fohlisch, Proc. Natl. Acad. Sci. USA **107**, 16772 (2010).
[17] P. Ganesh and M. Widom, Phys. Rev. Lett. **102**, 075701 (2009).
[18] V. V. Vasisht, S. Saw, and S. Sastry, Nat. Phys. **7**, 549 (2011).
[19] L. I. Aptekar, Sov. Phys. Dokl. **24**, 993 (1979).
[20] G. Monaco, S. Falconi, W. A. Crichton, and M. Mezouar, Phys. Rev. Lett. **90**, 255701 (2003).
[21] Y. Katayama, Y. Inamura, T. Mizutani, M. Yamakata, W. Utsumi, and O. Shimomura, Science **306**, 848 (2004).
[22] J. N. Glosli and F. H. Ree, Phys. Rev. Lett. **82**, 4659 (1999).
[23] M. Togaya, Phys. Rev. Lett. **79**, 2474 (1997).
[24] P. H. Poole, M. Hemmati, and C. A. Angell, Phys. Rev. Lett. **79**, 2281 (1997).
[25] H. E. Stanley and O. Mishima, Nature **396**, 329 (1998).
[26] P. H. Poole, F. Sciortino, U. Essmann, and H. E. Stanley, Nature **360**, 324 (1992).
[27] K. Murata and H. Tanaka, Proc. Natl. Acad. Sci. USA **112**, 5956 (2015).
[28] A. Cadien, Q. Y. Hu, Y. Meng, Y. Q. Cheng, M. W. Chen, J. F. Shu, H. K. Mao, and H. W. Sheng, Phys. Rev. Lett. **110**, 125503 (2013).
[29] K. Ling, H. Kim, M. Yoo, and S. Lim, Sensors **15**, 28154 (2015).
[30] N. B. Morley, J. Burris, L. C. Cadwallader, and M. D. Nornberg, Rev. Sci. Instrum. **79**, 56107 (2008).
[31] C. Ladd, J. So, J. Muth, and M. D. Dickey, Adv. Mater. **25**, 5081 (2013).
[32] Y. Lu, Q. Hu, Y. Lin, D. B. Pacardo, C. Wang, W. Sun, F. S. Ligler, M. D. Dickey, and Z. Gu, Nat. Commun. **6**, 10066 (2015).
[33] D. Morales, N. A. Stoute, Z. Yu, D. E. Aspnes, and M. D. Dickey, Appl. Phys. Lett. **109**, 91905 (2016).
[34] V. Y. Prokhorenko, V. V. Roshchupkin, M. A. Pokrasin, S. V. Prokhorenko, and V. V. Kotov, High Temp. **38**, 954 (2000).
[35] K. Suzuki and O. Uemura, J. Phys. Chem. Solids **32**, 1801 (1971).
[36] S. Yu and M. Kaviany, J. Chem. Phys. **140**, 64303 (2014).

[37] X. Zhao, X. Bian, J. Qin, Y. Liu, Y. Bai, X. Li, L. Feng, K. Zhang, and C. Yang, Europhys. Lett. **107**, 36004 (2014).
[38] X. Zhao, X. Bian, Y. Bai, and X. Li, J. Appl. Phys. **111**, 103514 (2012).
[39] A. P. Hammersley, S. O. Svensson, M. Hanfland, A. N. Fitch, and D. Hausermann, High Press. Res. **14**, 235 (1996).
[40] P. Juhás, T. Davis, C. L. Farrow, and S. J. L. Billinge, J. Appl. Crystallogr. **46**, 560 (2013).
[41] J. Blumm and J. Henderson, High Temp.-High Press. **32**, 109 (2000).
[42] L. W. Wang and Q. S. Mei, J. Mater. Sci. Technol. **22**, 569 (2006).
[43] J. Bednarcik, S. Michalik, M. Sikorski, C. Curfs, X. D. Wang, J. Z. Jiang, and H. Franz, J. Phys.: Condens. Matter **23**, 254204 (2011).
[44] D. W. Zhang, X. D. Wang, H. B. Lou, Q. P. Cao, L. W. Wang, D. X. Zhang, and J. Z. Jiang, J. Appl. Phys. **116**, 224903 (2014).
[45] W. G. Hoover, Phys. Rev. A **31**, 1695 (1985).
[46] S. Nose, J. Chem. Phys. **81**, 511 (1984).
[47] G. Kresse and J. Furthmuller, Phys. Rev. B **54**, 11169 (1996).
[48] P. E. Blöchl, Phys. Rev. B **50**, 17953 (1994).
[49] K. Georgarakis, L. Hennet, G. A. Evangelakis, J. Antonowicz, G. B. Bokas, V. Honkimaki, A. Bytchkov, M. W. Chen, and A. R. Yavari, Acta Mater. **87**, 174 (2015).
[50] L. H. Xiong, X. D. Wang, Q. Yu, H. Zhang, F. Zhang, Y. Sun, Q. P. Cao, H. L. Xie, T. Q. Xiao, D. X. Zhang, C. Z. Wang, K. M. Ho, Y. Ren, and J. Z. Jiang, Acta Mater. **128**, 304 (2017).
[51] Q. Yu, A. S. Ahmad, K. Ståhl, X. D. Wang, Y. Su, K. Glazyrin, H. P. Liermann, H. Franz, Q. P. Cao, D. X. Zhang, and J. Z. Jiang, Sci. Rep. **7**, 1139 (2017).
[52] J. L. Finney, Proc. R. Soc. A **319**, 479 (1970).
[53] J. L. Finney, Nature **266**, 309 (1977).
[54] P. J. Steinhardt, D. R. Nelson, and M. Ronchetti, Phys. Rev. B **28**, 784 (1983).
[55] P. Labastie and R. L. Whetten, Phys. Rev. Lett. **65**, 1567 (1990).
[56] J. P. Hansen and I. R. McDonald, *Theory of Simple Liquids* (Academic Press, London, 1986).